RSC Advances

ROYAL SOCIETY OF CHEMISTRY

www.rsc.org/advances

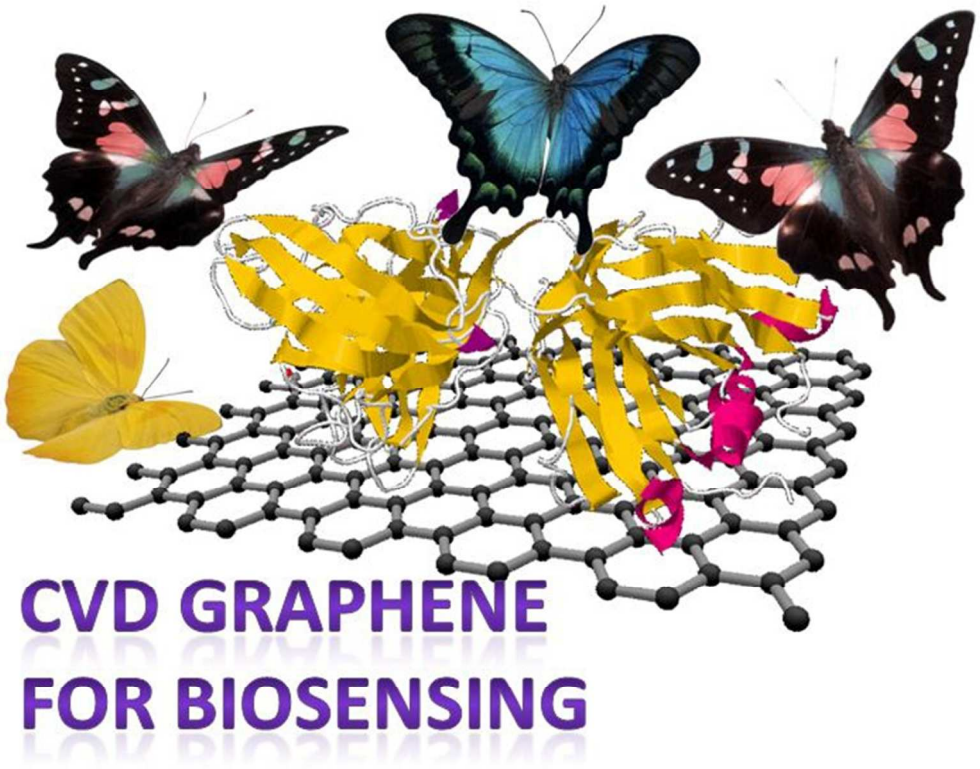

150x119mm (120 x 120 DPI)

Journal Name

RSCPublishing

ARTICLE

CVD graphene based Immunosensor

Cite this: DOI: 10.1039/x0xx00000x

Adeline Huiling Loo, Adriano Ambrosi, Alessandra Bonanni* and Martin Pumera*

Received ooth January 2012,
Accepted ooth January 2012

DOI: 10.1039/x0xx00000x

www.rsc.org/

Graphene synthesis by chemical vapour deposition (CVD) method has been receiving much attention from researchers. This is due to the fact that high quality graphene can be obtained at relatively low production costs. While there has been much advancement in CVD synthesis of graphene, little study has been done on the biosensing applications of CVD graphene. Herein, we aim to draw attention to employing CVD grown graphene as a potential platform for immunosensing of IgG. Using electrochemical impedance spectroscopy (EIS), we obtained a sensitive detection of rabbit IgG in the range of 0.1 – 100 $\mu g ml^{-1}$ with untreated CVD graphene as the electrode interface for direct immobilization of the recognition antibodies. From our report, it can be concluded that CVD grown graphene exhibits great potential to be utilized as a platform for immunosensing applications.

Introduction

Comprising of a single layer of carbon atoms that are densely packed in a honeycomb two-dimensional matrix, graphene has been the key interest of many researchers since its discovery in 2004.[1] The enormous attention which graphene is receiving is due to the extraordinary properties it displays. Examples of these properties include superior electron and thermal conductivity, robust mechanical strength and large surface area.[2-5] As a result of the above mentioned remarkable properties, graphene has also been dubbed as a "miracle material".[6] However, some of these mentioned outstanding properties can only be achieved by samples exhibiting the highest quality, such as mechanically exfoliated graphene.1 Presently, no graphene prepared via other techniques has demonstrated equivalent characteristics. Nevertheless, these synthetic methods are rapidly improving.

The methods for the preparation of graphene can be broadly categorized into two main approaches; bottom-up or top-down. For the instance of top-down approach, the working principle is based on stripping individual sheets of graphene from a graphite source material and this approach encompasses techniques such as oxidation of graphite to graphite oxide with subsequent thermal, chemical or electrochemical reduction, and mechanical or liquid-phase exfoliation of graphite.[7-9] On the other hand, for the case of bottom-up approach, the working principle is based on employing small carbon sources to fabricate graphene. The bottom-up approach comprises of epitaxial growth on silicon carbide[10] and chemical vapour deposition.[11]

In recent times, much effort has been channelled into research on graphene synthesis by chemical vapour deposition (CVD) method, which can generate high quality graphene with controlled number of layers and possibly at low mass production costs.[12] Although metal catalysts such as iridium, ruthenium, cobalt, platinum and iron have been successfully employed to grow graphene, nickel and copper represent the current most frequently adopted metal catalysts due to their lower cost and ease of controlling the number of graphene layers.[13-17] CVD grown graphene has been advantageously adopted for the fabrication of transparent electrodes, touch screens, and electronic devices.[18] This is in contrary to thermally/chemically reduced graphenes, which are of form of poweders. However, the use of CVD graphene for biosensing applications has not been fully explored yet. In particular, there have only been a few attempts on the utilization of CVD graphene as an electrochemical biosensing platform and these works include the detection of DNA hybridization and glucose sensing.[19-21] Till date, there has been no study conducted with the immunology systems.

Hence, in this work, electrochemical impedance spectroscopy (EIS) was employed to monitor the specific interactions between anti-rabbit IgG probes, which were immobilized on a CVD graphene platform, and rabbit IgG protein targets. A stable and uniform immobilization of the recognition element, anti-rabbit IgG, was achieved without any pre-treatment performed on the CVD graphene. In addition, a sensitive and specific detection of rabbit IgG protein, adopted as the model analyte, was obtained. Hence, this work demonstrates great promises for the future use of CVD grown graphene as a biosensing platform.

Experimental Section

Materials

Immunoglobulin G from rabbit serum (rabbit IgG), anti-rabbit immunoglobulin G produced in goat (anti-rabbit IgG), albumin from bovine serum (BSA), avidin, human hemoglobin, hydrochloric acid (conc. 37 %), sodium phosphate dibasic, sodium chloride, Tween® 20, potassium hexacyanoferrate (II) trihydrate and potassium hexacyanoferrate (III) were purchased from Sigma-Aldrich (Singapore).

Ultrapure water used in this study was obtained from a Milli-Q ion exchange column (Millipore) of resistivity 18.2 MΩ cm.

Buffer solutions used in this study are as follows: PBS (0.01 M phosphate, 0.135 M sodium chloride, pH 7.4), PBS-B (0.01 M phosphate, 0.135 M sodium chloride, 1 % BSA, pH 7.4) and PBS-T (0.01 M phosphate, 0.135 M sodium chloride, 0.05 % Tween® 20, pH 7.4).

Multilayer Graphene (105 nm thick on average) on Nickel Foil (CVD graphene) was purchased from Graphene Laboratories Inc. (Calverton, New York).

Equipment

All electrochemical measurements were conducted with a μAutolab type III electrochemical analyzer (Eco Chemie, Utrecht, The Netherlands) connected to a personal computer. Impedance measurements were controlled by NOVA software version 1.8 and recorded between 0.1 MHz and 0.1 Hz at a sinusoidal voltage perturbation of 10 mV amplitude. The obtained impedance spectra, presented as Nyquist plots in the complex plane, underwent electrochemical circle fitting. All electrochemical measurements were performed at room temperature with 10 mM $K_4[Fe(CN)_6]/K_3[Fe(CN)_6]$ (1 : 1 molar ratio) in PBS buffer solution as the redox probe, and Ag/AgCl as the reference electrode.

Raman spectra were acquired by using a confocal micro-Raman LabRam HR instrument (Horiba Scientific) in backscattering geometry with a CCD detector. A 514.5 nm Ar laser and a 100 X objective lens mounted on a Olympus optical microscope were employed for the focusing of the samples. The initial calibration was conducted at 0 and 520 cm^{-1} with a silicon wafer as the reference to give a peak position resolution of less than 1 cm^{-1}.

Scanning electron microscope images were attained by utilizing a JSM-7600F Schottky Field Emission Scanning Electron Microscope (JEOL, Japan) at 5 kV accelerating voltage.

Atomic force microscopy was performed with a MultiMode 8 atomic force microscope (Bruker, Singapore) controlled by Nanoscope 8.15 software and using the ScanAsyst mode.

X-ray photoelectron spectroscopy data were obtained with a Phoibos 100 spectrometer and an Mg X-ray radiation source (SPECS, Germany) for the measurement of wide-scan survey spectra and high-resolution N 1s spectra.

Procedures

Commercial CVD graphene was washed gently with ultrapure water before use.

Anti-rabbit IgG was immobilized onto the surface of CVD graphene by dry physical adsorption. 50 μl of anti-rabbit IgG in PBS buffer solution at a concentration of 100 μgml^{-1} was deposited onto CVD graphene and left to dry under the lamp for 30 minutes. Subsequently, the modified surface underwent gentle washings with PBS-T buffer solution, PBS buffer solution and ultrapure water to remove the excess anti-rabbit IgG that was not well adsorbed on the surface.

Subsequently, 50 μl of PBS-B buffer solution was next drop-cast on the anti-rabbit IgG modified CVD graphene surface and placed under the lamp for 10 minutes for drying. After which, gentle washings with PBS-T buffer solution, PBS buffer solution and ultrapure water were performed to remove the excess BSA which was not well adsorbed on the surface.

CVD graphene modified with anti-rabbit IgG and BSA then underwent incubation with rabbit IgG in PBS-T buffer solution. The incubation was performed at 37 °C for 1 hour in the oven. Finally, gentle washings with PBS-T buffer solution, PBS buffer solution and ultrapure water were performed to remove the excess of non-specifically adsorbed species. For selectivity study, negative controls were conducted using BSA, hemoglobin and avidin.

Results & Discussion

We investigate here the analytical proof-of-concept of performing immunosensing of IgG on CVD graphene. First of all, in order to gain a better understanding of the material employed as the sensing platform, characterizations by scanning electron microscopy (SEM), atomic force microscopy (AFM) and Raman spectroscopy were conducted with CVD graphene.

Characterization of CVD graphene was first performed with SEM to acquire information regarding its surface morphology. The SEM images obtained are shown in Figure S1 (Electronic Supplementary Information). Imaging of CVD graphene was carried out at two different magnifications of 370 × (Figure S1A) and 10 000 × (Figure S1B). From the SEM images, it can be observed that the CVD graphene, which was grown on nickel foil, demonstrates several grain boundaries between continuous islands of graphene. In addition, different colours ranging from white to dark grey, indicating regions with different number of graphene layers, can also be seen. Such observation is a common occurrence in samples grown on thin nickel films.[22] The homogeneous colour distribution, however, suggest a homogeneous graphene film thickness. Figure S1B clearly shows the edges of the graphene islands grown during the catalytic process. The edges are indicated by white lines which also account for folded graphene. On the other hand, the darker lines seen in Figure S1B may indicate structural discontinuity or cracks.

In order to gain more insights about the surface of the CVD graphene employed, AFM analysis was next conducted. Figure S2 (see SI) presents the AFM characterization of CVD graphene. The two-dimensional and three-dimensional profiles

of CVD graphene are depicted in Figures S2A and S2B respectively. From the two figures, it can be confirmed that several of the boundaries visible in SEM as white lines, resemble folded graphene sections which emerge from the film surface at a height of approximately 60 nm (Figure S2C).

Lastly, Raman spectroscopy was carried out to attain further structural information such as the presence of defects and the number of layers in CVD graphene. Figure S3 displays the Raman spectrum obtained in this study and it was noted that there is an absence of the D band (~ 1350 cm^{-1}) in the spectrum. This suggests that there is no significant presence of structural defects in the sp^2 lattice of CVD graphene. The average ratio of the intensity of G band (~ 1560 cm^{-1}) to 2D band (~ 2700 cm^{-1}) was calculated to be approximately 2.21. This implies that the CVD graphene is of multilayer structure.[23] Moreover, another piece of evidence which indicates the multilayer property is the slight shoulder observed at 2D band as single layer graphene will exhibit a symmetrical 2D band.[24]

Following the various characterizations, CVD graphene was employed as the transducing platform for the immunosensing of rabbit IgG by using electrochemical impedance spectroscopy (EIS) as the detection technique.[25] Scheme 1 illustrates the analytical protocol adopted. In summary, anti-rabbit IgG probes were first immobilized onto the surface of CVD graphene by physical adsorption. The successful attachment of anti-rabbit IgG probes onto CVD graphene was characterized by the appearance of a N 1s peak in X-ray photoelectron spectroscopy (XPS) study after the anti-rabbit IgG immobilization process (see Figure S4, supporting information). After which, BSA blocking was performed by drop-cast method in order to block off the remaining CVD graphene surface and deter non-specific binding. Lastly, incubation with rabbit IgG target was carried out. For each stage of the analytical procedure, impedance measurement was conducted and the respective Nyquist plots are shown in Scheme 1.

Briefly, bare CVD graphene demonstrated relatively the lowest charge transfer resistance as it was entirely accessible to the redox probe. Subsequently, anti-rabbit IgG probes were immobilized onto the surface of CVD graphene and the magnitude of charge transfer resistance increased owing to the decrease in accessibility of CVD graphene by the redox probe. After which, blocking of the remaining CVD graphene surface with BSA was performed and this further lowered the accessibility by redox probe and charge transfer resistance was further enhanced. Last of all, incubation with rabbit IgG, which binds specifically to anti-rabbit IgG, was carried out and it led to another increase in charge transfer resistance. This can be either attributed to the additional steric hindrance caused by the bulky rabbit IgG protein molecule, or the electrostatic interactions between rabbit IgG and redox probe.[26,27] It should be noted that in our previous article, we have compared physical adsorption, chemical linker and biotin/avidin linker for aptasensing on graphenes and we found that the highest sensitivity exhibits physical adsorption.[28]

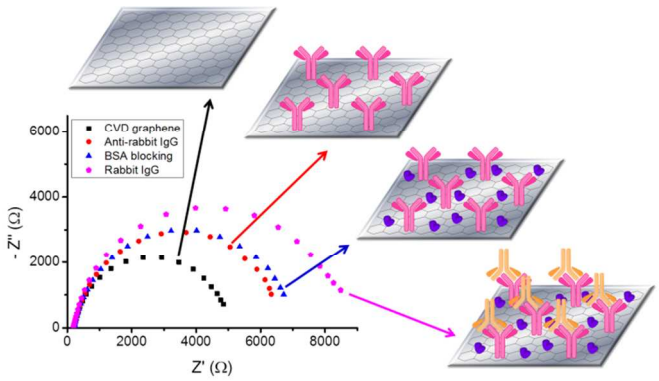

Scheme 1. Schematic illustration of the protocol and Nyquist plots (- Z'' vs. Z') of CVD graphene (black box), CVD graphene with immobilized anti-rabbit IgG (red circle), anti-rabbit IgG modified CVD graphene after BSA blocking (blue triangle) and anti-rabbit IgG modified CVD graphene after BSA blocking and incubation with rabbit IgG (pink pentagon). All measurements were performed with 10 mM $K_4[Fe(CN)_6]/K_3[Fe(CN)_6]$ in PBS buffer solution (pH 7.4) at room temperature with Ag/AgCl as reference electrode.

Selectivity is a fundamental requirement of a functional sensor. Hence, the selectivity performance of the proposed immunosensing platform was investigated by conducting negative control experiments with BSA, hemoglobin and avidin. The conclusions from the experiments are exemplified in Figure 1.

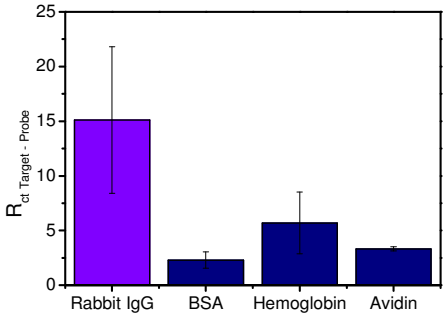

Figure 1. Illustration of the impedimetric response towards different protein. BSA, hemoglobin and avidin were employed as negative controls. Signal is represented as $R_{ct\ Target\ -\ Probe}$. The error bars correspond to replicate experiments. All measurements were performed with 10 mM $K_4[Fe(CN)_6]/K_3[Fe(CN)_6]$ in PBS buffer solution (pH 7.4) at room temperature with Ag/AgCl as reference electrode.

From Figure 1, it can be noticed that the impedimetric signal ($R_{ct\ Target\ -\ Probe}$) of rabbit IgG is much greater than that of the negative control proteins, BSA, hemoglobin and avidin. This indicates that the negative control proteins, BSA, hemoglobin and avidin, have negligible interactions with the immobilized anti-rabbit IgG probes. As such, the increase in charge transfer resistance after incubation with the negative control proteins is small, resulting in the low impedimetric signals. Therefore, the proposed immunosensing platform was deduced to be selective for rabbit IgG.

Subsequently, to assess the sensitivity of the proposed sensing system and to evaluate the range of detection, the variation of impedimetric signal with rabbit IgG concentration was examined. As depicted in Figure 2, the impedimetric signal increases with increasing concentration of rabbit IgG and the linear range of detection was determined to be from 0.1 to 100 μgml^{-1} with the limit of detection assessed to be 0.136 $\mu g\ mL^{-1}$.

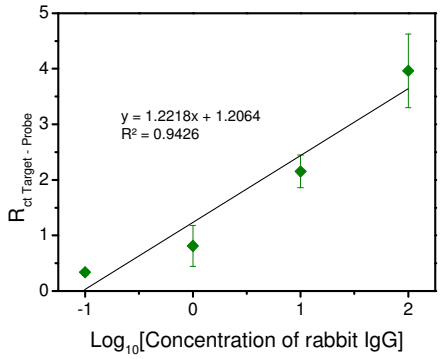

Figure 2. Impedimetric response towards different concentration of rabbit IgG. Signal is represented as $R_{ct\ Target\ -\ Probe}$. The error bars relate to replicate experiments. All measurements were performed with 10 mM $K_4[Fe(CN)_6]/K_3[Fe(CN)_6]$ in PBS buffer solution (pH 7.4) at room temperature with Ag/AgCl as reference electrode. Units of concentration: $\mu g\ ml^{-1}$.

With the selectivity and sensitivity aspects of the proposed sensing platform studied, we next move on to the optimization of the analytical protocol employed.

Anti-rabbit IgG optimization was carried out to establish the optimum concentration of the anti-rabbit IgG probe to be deposited onto the surface of CVD graphene in order to achieve best surface coverage. Impedance measurements were performed for a series of anti-rabbit IgG concentration and the spectra acquired were analysed and displayed as histograms shown in Figure 3.

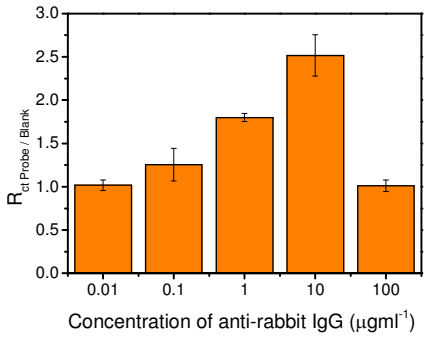

Figure 3. Comparison of impedimetric response towards different concentration of anti-rabbit IgG. Signal is represented as $R_{ct\ Probe\ /\ Blank}$. The error bars correspond to replicate experiments. All measurements were performed with 10 mM $K_4[Fe(CN)_6]/K_3[Fe(CN)_6]$ in PBS buffer solution (pH 7.4) at room temperature with Ag/AgCl as reference electrode.

As exhibited in Figure 3, the impedimetric signal ($R_{ct\ Probe\ /\ Blank}$) increases progressively as the concentration of anti-rabbit IgG increases from 0.01 to 10 μgml^{-1}. Note that the concentration of IgG in human serum and plasma samples is 4-16 mg mL^{-1} which is fully compatible with linear range of calibration presented here. However, when the concentration of anti-rabbit IgG further increases to 100 μgml^{-1}, a decrease in the signal can be observed. A higher impedimetric signal correlates to a greater amount of anti-rabbit IgG being successfully immobilized onto the surface of CVD graphene. For that reason, 10 μgml^{-1} is determined to be the optimum concentration of anti-rabbit IgG to be deposited onto the surface of CVD graphene as it ensures the greatest coverage of the surface. The previous research on chemically reduced graphenes exhibited poorer performance, with detection range of 0.3 - 7 $\mu g\ ml^{-1}$.[29] In addition, here we compare the selectivity with BSA, hemoglobin and avidin while previously the comparison of selectivity was done only with BSA.[29] The advantage of CVD graphene is that it is transparent and it can be easily integrated to transparent electronic devices.

In addition, in order to ensure that the physiological pH (7.4) employed for the EIS measurements was suitable for the proposed immunosensing concept, a pH dependent EIS study was conducted (see Figure S5, Supporting Information). From the obtained results, it can be confirmed that pH 7.4 is the most appropriate pH to be utilized for this study.

Last of all, the stability of the fabricated immunosensor was assessed by performing a stability study over a time period of

seven days (see Figure S6, Supporting Information). The results indicate that after seven days, the recorded signal decrease was 48 % with an increase in the % RSD value.

Conclusions

In summary, we have demonstrated in this study the proof-of-principle of performing immunosensing of IgG on CVD graphene. The proposed sensing concept was shown to be selective for IgG, with good discrimination from hemoglobin, avidin and BSA. Furthermore, the linear range of detection was determined to be from 0.1 to 100 μgml^{-1}, thereby conferring reasonable sensitivity to the proposed system. Probe optimization study concluded that 10 μgml^{-1} is the optimum concentration of anti-rabbit IgG to be deposited on the surface of CVD graphene. CVD graphene based immunosensors should find their way into the biomedical application in near future.

Notes

Authors address

Division of Chemistry & Biological Chemistry, School of Physical and Mathematical Sciences, Nanyang Technological University, Singapore 637371.

Corresponding authors

pumera@ntu.edu.sg
a.bonanni@ntu.edu.sg

References

1 K. S. Novoselov, A. K. Geim, S. V. Morozov, D. Jiang, Y. Zhang, S. V. Dubonos, I. V. Grigorieva and A. A. Firsov, *Science*, 2004, **306**, 666 – 669.

2 K. S. Novoselov, A. K. Geim, S. V. Morozov, D. Jiang, M. I. Katsnelson, I. V. Grigorieva, S. V. Dubonos and A. A. Firsov, *Nature*, 2005, **438**, 197 – 200.

3 M. Pumera, *Mat. Today,* 2011, **14**, 308.

4 N. A. Kotov, *Nature*, 2006, **442**, 254 – 255.

5 C. Lee, X. D. Wei, J. W. Kysar and J. Hone, *Science*, 2008, **321**, 385 – 388.

6 K. S. Novoselov, V. I. Fal'ko, L. Colombo, P. R. Gellert, M. G. Schwab and K. Kim, *Nature*, 2012, **490**, 192 – 200.

7 P. Blake, P. D. Brimicombe, R. R. Nair, T. J. Booth, D. Jiang, F. Schedin, L. A. Ponomarenko, S. V. Morozov, H. F. Gleeson, E. W. Hill, A. K. Geim and K. S. Novoselov, *Nano Lett.*, 2008, **8**, 1704 – 1708.

8 Y. Hernandez, V. Nicolosi, M. Lotya, F. M. Blighe, Z. Sun, S. De, I. T. McGovern, B. Holland, M. Byrne, Y. K. Gun'Ko, J. J. Boland, P. Niraj, G. Duesberg, S. Krishnamurthy, R. Goodhue, J. Hutchison, V. Scardaci, A. C. Ferrari and J. N. Coleman, *Nat. Nanotechnol.*, 2008, **3**, 563 – 568.

9 D. R. Dreyer, S. Park, C. W. Bielawski and R. S. Ruoff, *Chem. Soc. Rev.*, 2010, **39**, 228 – 240.

10 I. Forbeaux, J. M. Themlin and J. M. Debever, *Phys. Rev. B*, 1998, **58**, 16396 – 16406.

11 L. Chen, Y. Hernandez, X. Feng and K. Müllen, *Angew. Chem. Int. Edit.*, 2012, **51**, 7640 – 7654.

12 X. Li, W. Cai, J. An, S. Kim, J. Nah, D. Yang, R. Piner, A. Velamakanni, I. Jung, E. Tutuc, S. K. Banerjee, L. Colombo and R. S. Ruoff, *Science*, 2009, **324**, 1312 – 1314.

13 P. W. Sutter, J.-I. Flege and E. A. Sutter, *Nat. Mater.*, 2008, **7**, 406 – 411.

14 A, Ambrosi, A. Bonanni, Z. Sofer, M. Pumera, *Nanoscale*, 2013, **5**, 2379.

15 J. Coraux, A. T. N'Diaye, C. Busse and T. Michely, *Nano Lett.*, 2008, **8**, 565 – 570.

16 V. Roumen, M. Alexander, H. P. Roumen, K. Raymond, M. Myrjam, V. Annick and H. Chris Van, *Nanotechnology*, 2010, **21**, 095602.

17 D. Kondo, S. Sato, K. Yagi, N. Harada, M. Sato, M. Nihei and N. Yokoyama, *Appl. Phys. Express*, 2010, **3**, 025102.

18 A. Ambrosi, M. Pumera, *J. Phys. Chem. C* 2013, **117**, 2053.

19 A. Gutés, C. Carraro and R. Maboudian, *Biosens. Bioelectron.*, 2012, **33**, 56 – 59.

20 S.-R. Guo, J. Lin, M. Penchev, E. Yengel, M. Ghazinejad, C. S. Ozkan and M. Ozkan, *J. Nanosci. Nanotechno.*, 2011, **11**, 5258 – 5263.

21 Y. H. Kwak, D. S. Choi, Y. N. Kim, H. Kim, D. H. Yoon, S.-S. Ahn, J.-W. Yang, W. S. Yang and S. Seo, *Biosens. Bioelectron.*, 2012, **37**, 82 – 87.

22 K. S. Kim, Y. Zhao, H. Jang, S. Y. Lee, J. M. Kim, K. S. Kim, J.-H. Ahn, P. Kim, J.-Y. Choi and B. H. Hong, *Nature*, 2009, **457**, 706 – 710.

23 A. C. Ferrari, *Solid State Commun.*, 2007, **143**, 47 – 57.

24 A. C. Ferrari, J. C. Meyer, V. Scardaci, C. Casiraghi, M. Lazzeri, F. Mauri, S. Piscanec, D. Jiang, K. S. Novoselov, S. Roth and A. K. Geim, *Phys. Rev. Lett.*, 2006, **97**, 187401.

25 A. Bonanni, A. H. Loo and M. Pumera, *TrAC, Trends Anal. Chem.*, 2012, **37**, 12 – 21.

26 J. S. Daniels and N. Pourmand, *Electroanal.*, 2007, **19**, 1239 – 1257.

27 E. Katz and I. Willner, *Electroanal.*, 2003, **15**, 913 – 947.

28 A. H. Loo, A. Bonanni, M. Pumera, *Chem. Asian J.* 2013, **8**, 198–203.

29 A. H. Loo, A. Bonanni, A. Ambrosi, H. L. Poh, M. Pumera, *Nanoscale* 2012, **4**, 921.

